Effect of confinement on dynamics and rheology of dilute DNA solutions. I. Entropic spring force under confinement and a numerical algorithm

Nathanael J. Woo

Scientific Computing / Computational Mathematics Program, Stanford University, Stanford, California 94305

Eric S. G. Shaqfeh[a)]

Departments of Chemical and of Mechanical Engineering, Stanford University, Stanford, California 94305

Bamin Khomami

Department of Chemical Engineering and Materials Research Laboratory, Washington University, St. Louis, Missouri 63130

(Received 20 March 2003; final revision received 17 December 2003)

Synopsis

We present the effect of confining walls on the rheology and dynamics of dilute polymeric solutions using a self-consistent multiscale simulation technique. In Part I we formulate the mathematical problem necessary to understand and model these dynamics. Various polymer models (the Kramers' freely jointed bead-rod chain, FENE, worm-like, and inverse Langevin chains) are used to describe the polymer chain dynamics based on their success in previous studies [H.P. Babcock *et al.*, Phys. Rev. Lett. 85, 2018 (2000); J. S. Hur *et al.*, J. Rheol. **44**, 713 (2000); **45**, 421 (2001)]. Theoretical arguments suggest that the main consequences of confinement on chains are (a) the entropic force law is altered due to the loss of chain configurational space and (b) the viscous drag on the chain is increased due to *hydrodynamic interactions with the wall*. In this study, the correct entropic spring force law in the presence of confining walls is developed. In addition, an efficient multiscale simulation technique for modeling the dynamics of bead-spring models with the force law is reported. © *2004 The Society of Rheology.* [DOI: 10.1122/1.1648642]

I. INTRODUCTION

There are many important natural and industrial processes in which suspensions are confined within domains comparable to the size of the suspended particles, i.e., blood flow through small capillaries and chromatographic separation through porous media. More recently, the use of microchannels in micro-electro-mechanical system (MEMS) devices for transport and chemical analysis of pharmaceuticals has attracted significant interest since the microscale size of such devices requires only a minute amount of expensive chemicals for analysis thus potentially replacing conventional pharmaceutical laboratories. Typically many devices of different functionality connected by channels and

[a)]Author to whom correspondence should be addressed; electronic mail: eric@chemeng.stanford.edu

gates are etched on a single-lab-on-a-chip. The multifunctionality of the devices allows a series of automated experiments and analysis to be carried out with ease [Ho and Tai (1996, 1998); Lee *et al.* (2001)].

One area of application directly relevant to our study is transport and sequencing of DNA in MEMS devices. In typical MEMS devices, the channel size is about 10 μm, for example, while λ-phage DNA has a radius of gyration (Rg) on the order of 1 μm and a contour length of 21 μm [Ho and Tai (1998); Smith *et al.* (1999)]. In such systems where the size of the chain is comparable to the channel size, the effect of the confining wall is very important and the rheology and chain dynamics are greatly affected.

The consequences of confinement on dilute solution rheology have been considered in a number of other studies [Brunn (1976); Aubert and Tirrel (1982); Brunn and Grisafi (1987); Muller-Mohnssen *et al.* (1990); Ausserre *et al.* (1991); Mavrantzas and Beris (1992); Schiek and Shaqfeh (1995); Chopra and Larson (2002)]. It has been shown that, near the boundary, there exists a region called a *depletion layer* where chain segments are depleted due to excluded volume interaction with the wall. Therefore the chain concentration varies from zero at the wall to its bulk value over the length scale of this depletion layer. This variation in concentration is coupled to variation in other quantities such as the force density and velocity profile.

The first direct experimental verification of the existence of such a depletion layer and its effect on bulk rheology was demonstrated by Muller-Mohnssen *et al.* (1990) and Ausserre *et al.* (1991). Muller-Mohnssen *et al.* (1990) used a laser-differential microanemometer (LMA) to obtain the velocity of polyacrylamide (PAM) solutions near the wall and Ausserre *et al.* (1991) used an evanescent-wave-induced fluorescence (EWIF) technique to obtain the depletion layer thickness of a dilute rod-like Xanthan gum solution in shear flow. Different results were obtained depending on the flexibility of the chain. For rod-like polymers, Ausserre *et al.* found the depletion layer was an increasing function of the shear rate. Their experimental observation was confirmed by numerical simulations [de Pablo *et al.* (1992)], which showed slight shear-thinning before the onset of shear thickening of the depletion layer.

On the other hand, for flexible polymers the depletion layer was found to always be shear thinning [Duering and Rabin (1990, 1991)]. Early work [Brunn (1976); Aubert and Tirrel (1982); Brunn and Grisafi (1987)] modeled the flexible polymer in confined geometries as a Hookean dumbbell that interacted repulsively with the wall. They found the same qualitative result that in the center of the channel the velocity was linear and decreased rapidly from its bulk value to zero at the wall over a molecularly small length scale. Thus, overall, there was a nonlinear velocity profile.

Mavrantzas and Beris (1992) constructed a Hamiltonian for a Hookean dumbbell and by minimizing the Helmholtz free energy found the same general trend found by others. More recently, they refined their formulation to account for the effect of the wall on the Gaussian probability distribution function [Mavrantzas and Beris (1999)], thereby correcting their chain density profile near the wall. In contrast to previous work [Duering and Rabin (1990); Mavrantzas and Beris (1992)], they found that at higher shear rates the depletion layer increased near the wall.

All the investigators mentioned above, who considered flexible chains, used the Hookean dumbbell model and confirmed the earlier results of Brunn (1976) that there exists a region near the wall where the field variables change rapidly and chains are depleted. Brunn (1976) observed that the length of the region where such rapid variation occurred was the end-to-end distance of the Hookean dumbbell. In Part II of this study, we connect the depletion layer thickness to the configurational dispersion layer thickness

in shear flow in the absence of the wall [Chopra and Larson (2002); Hur *et al.* (2000)] and obtain large gap width asymptotic scalings for the effective viscosity which is applicable to both flexible chains and rigid rods.

As stated above, most prior studies employed a very simplified polymer model for flexible polymers assuming linear velocity fields. However, in this study, we perform self-consistent flow simulations. We also employ more realistic models for flexible polymers including bead-rod and nonlinear bead-spring models. These models have been employed in our simulation because of their success in describing the dynamics of λ-phage DNA under bulk flow [Babcock *et al.* (2000); Hur *et al.* (2000, 2001)]. Thus our focus is to study the physics of dilute λ-phage DNA solutions under confinement. As will be shown in due course, special care must be taken when using coarsely grained bead-spring models for flow in highly confined geometries. Finally, in contrast to previous studies that have only considered excluded volume interaction, we have included hydrodynamic interaction with the wall in our analysis and have shown that the interaction is essential for an accurate description of the rheology of thin gap flow. On the other hand, we have ignored both interchain and intrachain hydrodynamic interactions in our analysis since it has been shown that for both dilute and semidilute λ-phage DNA solution they are unimportant [Hur *et al.* (2001)]. In this paper, we develop a general mathematical formulation and numerical technique to simulate λ-phage DNA solutions in microchannel flow. In Part II we discuss the effect of confinement on the effective rheology of the DNA solutions and the chain dynamics.

II. SIMULATION METHOD

A. Polymer models

The most finely grained model that we employ for the flexible polymer (or DNA) is the freely jointed bead-rod chain in which beads are connected by rods constrained to maintain successive beads at a uniform distance. This rod length corresponds to a Kuhn length (a) which is the smallest rigid length scale of the polymer when there are no excluded volume effects [Graessley *et al.* (1999)]. Therefore the number of Kuhn steps in a chain is the measure of the flexibility of the chain and a longer chain or, equivalently, finer discretization, is required to model a more flexible chain.

The Brownian dynamics simulation technique we employ for bead-rod chains was discussed by Liu (1989) and Doyle *et al.* (1997a) for the case of constant drag and we refer the readers to these papers for more details. The algorithm for bead-spring models with configuration dependent drag is discussed in Sec. IV.

The stochastic differential equation for the freely jointed chain model is given by

$$dr_i^v = \left(\frac{\partial u_i^\infty}{\partial x_j} r_j^v + \frac{1}{\xi} F_i^{\mathrm{con},v} \right) dt + \sqrt{\frac{2kT}{\xi}}\, dW_i^v , \tag{1}$$

where ξ is the drag on the bead, r_i^v is the position of the vth bead, $F_i^{\mathrm{con},v}$ is the constraint force necessary to maintain beads of the chain at a constant distance (Kuhn length a), u_i^∞ is the undisturbed solvent velocity, and dW_i^v is the Wiener process which satisfies the fluctuation-dissipation theorem [Öttinger (1996)]. For bead-spring models, we use the entropic spring force $F_i^{\mathrm{sp},v}$ instead of $F_i^{\mathrm{con},v}$ in Eq. (1) [Somasi *et al.* (2002)]. DNA chains follow the worm-like spring force law proposed by Marko and Siggia (1995), given by

$$\frac{F_{3D}^{WLC}\lambda}{kT} = \frac{1}{4(1-Q)^2} - \frac{1}{4} + Q, \tag{2}$$

where λ is the persistence length of the chain and is equal to half of Kuhn length a. This spring law is supported by a comparison to experiments where force measurements of a single stretched DNA chain were made [Smith *et al.* (1992)]. Other commonly used spring force laws include the inverse Langevin chain (ILC) and FENE and they are discussed in detail elsewhere [Woo (2003)]. The ILC chain follows the following force law:

$$\frac{F_{3D}^{ILC}a}{kT} = \frac{Q(3-Q^2)}{1-Q^2}. \tag{3}$$

B. Two-dimensional bead-spring models

1. Freely jointed chain in two dimensions

Here we derive a two-dimensional (2D) force law for the freely jointed chain (FJC) and the worm-like chain (WLC). For our confined flow between two walls, as the gap width approaches zero, the force law governing the chains in three dimensions (3D) becomes the 2D force law. As we shall see, this difference is important for chains confined below $2Rg$ (radius of gyration). In another context, chains electrostatically absorbed onto lipid bilayers are best modeled as 2D chains [Maier and Radler (1999); Muthukumar (1999)].

For freely jointed chains, one can construct the partition function to find the average extension as a function of the force applied [Rowley (1994)]. Since detailed discussion can be found elsewhere [Woo (2003)], we skip intermediate steps and report the final result for extension as a function of entropic spring force:

$$Q = \frac{I_1(Fa/kT)}{I_0(Fa/kT)}, \tag{4}$$

where $I_0(x)$ and $I_1(x)$ are the modified Bessel functions of first kind [Abramowitz and Stegun (1984)]. We define the ratio of these two Bessel functions as $I_{1/0}(x) = I_1(x)/I_0(x)$, and inverting to express the force in terms of extension, we obtain

$$\frac{F_{2D}^{FJC}a}{kT} = I_{1/0}^{-1}(Q). \tag{5}$$

A Padé approximation to this force law can be obtained by matching the two limiting cases at low and high extension and we obtain

$$\frac{F_{2D}^{FJC,\ Pade}a}{kT} = \frac{Q(2-Q^2)}{1-Q^2}. \tag{6}$$

We also consider lateral chain fluctuation, which denotes the characteristic chain extension perpendicular to the fully extended ($Q \approx 1$) chain orientation and can be estimated to be $1-Q^2$. We find

$$\langle t_\perp^2 \rangle \sim \frac{1}{2F}, \tag{7}$$

which is 1/2 the lateral fluctuation in 3D. This is consistent with the fact that there is only one lateral direction in 2D whereas there are two directions in 3D. This fact will be useful for derivation of the worm-like chain force law in 2D.

2. Worm-like chain in 2D

Following Marko and Siggia (1995), we consider a chain fully extended near its maximum extension. The lateral fluctuation in chain length $t_\perp$ can be estimated as

$$\langle t_\perp^2 \rangle \sim \frac{1}{2(F\lambda)^{1/2}}, \tag{8}$$

where λ is the persistence length of the DNA and F is the force required to hold its end-to-end distance at a certain extension Q. The average fluctuation in the 2D chain is 1/2 that in 3D since there is only one lateral direction in 2D. For small lateral fluctuations we can write

$$Q \sim 1 - \frac{\langle t_\perp^2 \rangle}{2} \sim 1 - \frac{1}{(16F\lambda)^{1/2}}. \tag{9}$$

By rearranging terms and solving for the force we obtain

$$F\lambda \sim \frac{1}{16(1-Q)^2}. \tag{10}$$

At small extension, we necessarily need to recover the Hookean force law $F = 2Q$ (cf. $F = 3Q$ in 3D). Therefore by matching the two limits we obtain the following expression for a worm-like chain in 2D:

$$\frac{F_{2D}^{WLC}\lambda}{kT} = \frac{1}{16(1-Q)^2} - \frac{1}{16} + \frac{7Q}{8}. \tag{11}$$

As will be shown in Sec. III, confinement by the impenetrable walls changes the force law and it correctly becomes the 2D force law within the limit of small gap width. Therefore use of the 3D force law in such geometries results in significant errors. In this paper, we use a new algorithm to calculate the correct force law in a general two wall confined channel by using the method of reflection [Woo (2003)].

C. Momentum equation

In Part II of this study, we consider the chain dynamics in two model planar flow, namely, shear and Poiseuille flow. In shear flow, the upper plate is maintained at a constant velocity U relative to the lower plate separated by gap width H. The flow direction is denoted by x and the gradient direction by y. In the absence of polymers in the solution, a linear Newtonian velocity profile develops across the channel. For Poiseuille flow, in the absence of the polymers, the velocity profile becomes parabolic. However in the presence of polymers, the polymer chains exert extra force on the mixture of Newtonian fluid and other chains and the channel velocity deviates from its Newtonian profile. The resulting momentum equation is

$$\eta_s \frac{d^2\langle u_x \rangle}{dy^2} - \frac{dP}{dx} + \langle f_x \rangle = 0, \tag{12}$$

where the force density $\langle f_x(y)\rangle = \langle \rho(y) F_x^{\mathrm{hyd}}(y)\rangle$ is the average force exerted on the mixture by the polymer chain segments. The chain segmental density profile across the channel $\rho(y)$ and hydrodynamic force on the chain segment in the direction of flow (x component) F_x^{hyd} are obtained from Brownian dynamics simulation. The momentum equation [Eq. (12)] is discretized in the y direction (the flow gradient direction) and the velocity is solved by a finite difference scheme.

Since the force density is a functional of velocity, to obtain the self-consistent velocity profile, the momentum equation is solved iteratively. To start the iteration, Newtonian velocity is assumed and Brownian dynamics are performed. From this simulation we obtain the force density profile. By integrating the momentum equation [Eq. (12)] using this force density gives the next iterate of the velocity. This iterative process is repeated until successive velocity profiles differ by less than some prescribed tolerance. We find about three iterations are sufficient for convergence of the nonlocal velocity profile to within 1%. This self-consistent mean-field approach has been successfully used elsewhere and was shown to be a very good approximation [Koch and Brady (1986); Doyle *et al.* (1997b)].

It is appropriate here to highlight one of the important dimensionless parameters that will appear often in discussion of our results. The flow strength is characterized by the Weissenberg number which is defined as $Wi = \tau\dot{\gamma}$, where τ is the longest relaxation time of the DNA chain in the bulk solution and $\dot{\gamma}$ is the applied shear rate averaged over channel gap width H. For shear flow, $\dot{\gamma}$ is equal to the wall shear rate U/H. The longest relaxation time is obtained from simulation by stretching the chain to its full contour length and subsequently allowing it to relax in the bulk. The long time decay of the stress is fit to a single exponential to give the *longest relaxation* time of the chain. For Kramers chains in 3D, Doyle *et al.* (1997a) found $Wi = 0.0142N^2\dot{\gamma}\xi a^2/kT$, where N is the number of Kuhn steps in the chain, and a is the Kuhn length.

III. FORCE LAWS IN THIN GAPS

A. Problems with the use of 3D bulk spring force law in thin gaps

In 3D bulk simulations, bead-spring models have been successful in capturing both the microscopic polymer chain conformations as well as the macroscopic material properties if a suitable number of springs is used to model the chain [Herrchen and Öttinger (1997); Babcock *et al.* (2000); Hur *et al.* (2000)]. For freely jointed chains, the representative spring force can be derived from statistical mechanics [Kuhn and Grün (1942); Marko and Siggia (1995); Doyle *et al.* (1997a)], and in general for 3D bead-spring models, each spring represents roughly 10 or more Kuhn steps and captures the equilibrium statistics of the end-to-end vector of the chain segment that the spring represents. The preference of bead-spring models over bead-rod models in complex fluid calculations is primarily due to the high computational cost associated with bead-rod calculations. An added difficulty, in the present case of flow in a confined geometry, is the increased computational cost in resolving variations in the direction normal to the confining walls.

To accurately develop a bead-spring model for polymers in confined geometries, one must realize that the presence of the impenetrable walls breaks the isotropic nature of the random walk of the chain and as a result there exist different entropic chain restoring forces in the directions normal and tangent to the confining walls. The region where chain segments reside is described by an ellipsoid where the foci are the two ends of the chain. If one were to simulate chains confined in narrow gaps, in the case where this ellipsoid touches either of the confining walls, the configurational space changes from that characterized by a 3D unhindered random walk to that of a hindered random walk. Thus one

has to use either a bead-rod model for the chain, which will correctly account for the effect of the change in configurational space created by the walls, or use a bead-spring model which uses a corrected entropic spring force law that differs from the unconfined force law.

In the present study in which we solve the momentum equation [Eq. (12)], correct evaluation of the force density $\langle f_x \rangle$ plays a crucial role in obtaining the correct average flow fields and the effective rheology. To summarize, the use of 3D entropic force law in a confined geometry is incorrect for the following reasons: (a) an inaccurate description of the entropic force parallel to the confining walls ($F_{\parallel}$) and (b) an inaccurate chain density profile near the wall, which is related to the entropic force perpendicular to the confining walls ($F_{\perp}$).

Corrections to the probability distribution induced by wall confinement were considered by Mavrantzas and Beris (1999) using the Hookean dumbbell model to correct the density profile in the gap. But since they used the linear model for the spring, no change in force parallel to the confining walls occurs and their spring force does not approach the correct 2D limit as the gap width decreases. Shown in Fig. 1 are the chain segmental density profile and force density profile as a function of the gap width at $Wi = 10$ calculated using the algorithm discussed in Sec. IV (with constant drag on the bead). The use of the 3D entropic force law causes overprediction of the chain segmental density near the wall and the shape of the force density is different compared to the Kramers bead-rod chain. If one uses more a finely grained model (i.e., one with more modes in the bead-spring chain), the chain density profile improves since a more finely grained model better mimics the random walk of the bead-rod chain in the presence of the wall.

B. Effect of one wall on the entropic spring force law

The probability of going from point A to point B in the *presence* of the wall (Fig. 2) is equal to the probability of going from point A to point B minus the probability of going from point A to point B^* (which is a mirror image of point B) with both probabilities in the *absence* of the wall [Feller (1961)]. Any point reaching a point on the wall C has zero probability and the wall serves as an *obsorbing* barrier that repels the chain [DiMarzio (1965); Allegra and Colombo (1993)]. The wall is said to be *absorbing* if the probability is zero at the wall, whereas it is said to be *reflecting* if the gradient of probability is zero at the wall. Therefore the probability of finding end-to-end vector Q fixed at points A and B is, apart from the normalization factor, given by

$$P_w(Q) = P(Q) - P(Q_{-1}), \tag{13}$$

where Q_{-1} is the end-to-end vector between points A and B^* [Fig. 5(a)].

The entropic force acting on point A is then

$$F_w(Q) = -kT \frac{\partial \ln P_w(Q)}{\partial Q}. \tag{14}$$

By rearranging terms we have the following expression for force in the presence of one wall in terms of the force and probability in the absence of the wall:

$$F_w(Q) = F(Q) + P(Q_{-1}) \left[\frac{F(Q) - F(Q_{-1})}{P(Q) - P(Q_{-1})} \right]. \tag{15}$$

Shown in Fig. 3(a) is the chain extended *parallel* to the confining walls, where ϵ denotes the distance between the chain and the lower wall. Here in Sec. III B we will assume the upper wall is at least a chain's contour length away from the chain and

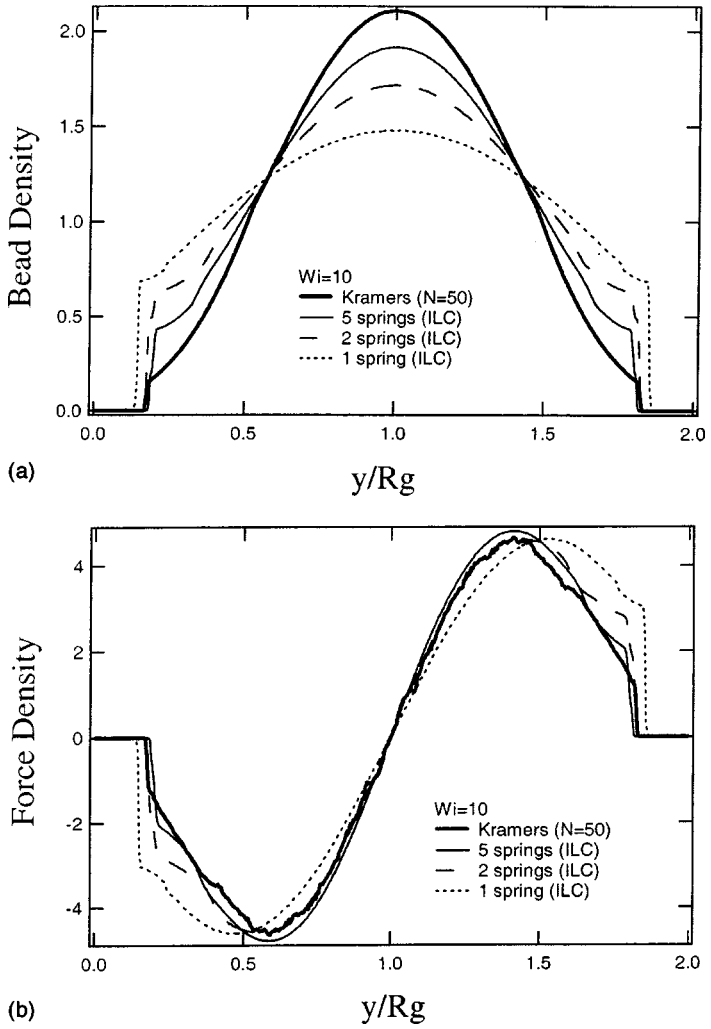

FIG. 1. Chain segment density profile (a) and force density profile (b) at $Wi = 10$ and gap width $H = 2Rg$ using uncorrected 3D ILC spring force law compared to those of the exact Kramers chain. The effect of coarse graining on the profile is shown at three different discretizations (one, two, and five springs).

therefore the chain does not *feel* the presence of the upper wall. Only the lower wall will be close enough to interact with the chain. In Sec. III C we will consider the case where both the upper and lower walls are near the chain. For chains very near the lower wall, one can find the entropic spring force in a series expansion of small ϵ and we define the correction factor to the 3D force as $f = (F_w - F_{3D})/F_{3D}$. Here F_{3D} denotes the 3D entropic spring force required to maintain separation of Q. After substituting Eq. (3) and its probability distribution function into Eq. (15) it can easily be shown that for force in the direction parallel to the wall ($F_\parallel$), $f = -4/9N$ for small extensions and $f = -1/N$ for large extensions. Since for λ-phage DNA N is about 150 and for typical flexible polymers N is much larger, the correction factor is negligible and we recover the 3D force within the limit that ϵ goes to zero and N goes to infinity. When chains are very

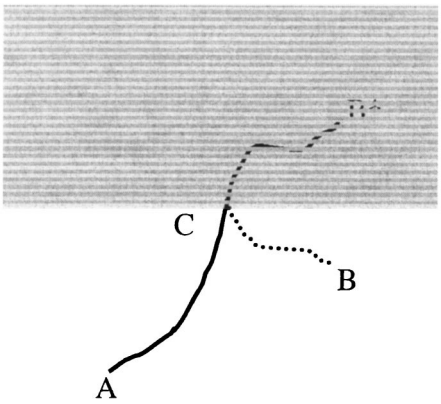

FIG. 2. Probability of having random walk from point A to B in the presence of the wall expressed in terms of the difference in probability of having random walk from point A to B and from point A to B^* (which is a mirror image of B).

near the wall, the configurational space is reduced to exactly half that in 3D. Since the *distribution* of the chain configurations allowed remains the same, $F_{\|}$ remains the same as the 3D force.

On the other hand, when one considers the force *perpendicular* to the confining walls ($F_{\perp}$) where the chain is still stretched in the direction parallel to the confining walls [Fig. 3(a)], unlike the 3D force which is identically zero due to symmetry, there is a nonzero force pushing the chain away from the lower wall due to the lower probability of finding chain segments between the lower wall and the lower bead. In this case $f = 1/N\epsilon$ for small extensions, and $f = 1/\epsilon^2$ for large extensions. Therefore even though the extension is small, the chain can experience very large force near the lower wall perpendicular to the walls and this results in a lower chain segmental density profile near the wall.

Similarly, for the chains extended perpendicular to the confining walls shown in Fig. 3(b), $f = -1/2N$ for large extensions and $f = -1/NQ$ for small extensions for force perpendicular to the confining walls ($F_{\perp}$). For most cases the correction is negligible, but for small extensions with small N, the correction factor can be significant. For example, for Kramers chain of $N = 10$, the correction factor becomes large in magnitude and the force on the upper bead, which is further away from the wall, actually reverses its direction and points away from the wall and away from the other bead instead of pointing toward the wall as shown in the lower left corner of Fig. 4. Although not shown in Fig.

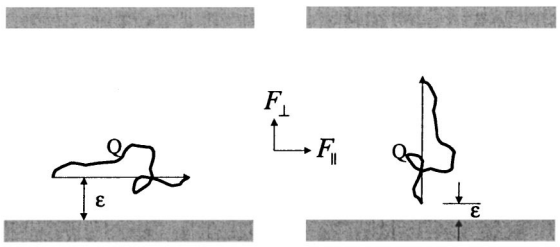

FIG. 3. Entropic spring force for chain extension Q extended parallel or perpendicular to the confining walls.

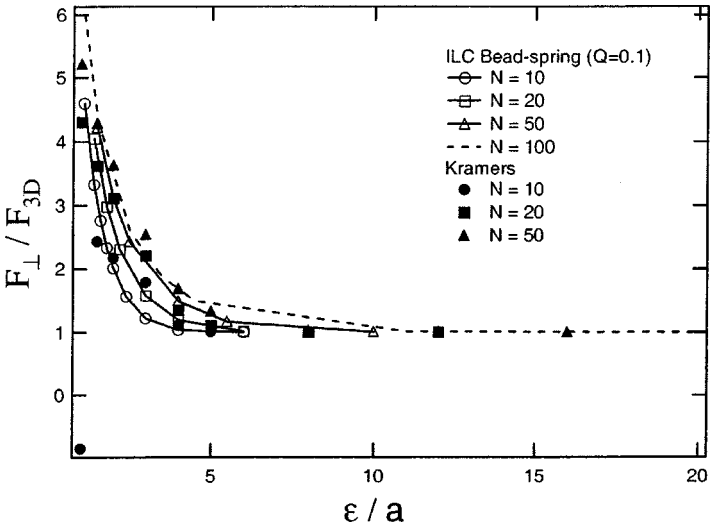

FIG. 4. Comparison of bead-rod force law with bead-spring force at extension $Q = 0.1$ as a function of ϵ for chains oriented perpendicular to the confining walls. For small chain size, the force reverses direction and points away from the wall due to the presence of the wall (note the data point in the lower left corner for $N = 10$).

4, the bead-spring models reverse the direction of force eventually at lower ϵ. For most ϵ, we find quantitatively good agreement between Eq. (15) of the bead-spring model and the bead-rod model.

The disagreement between the bead-spring model and the bead-rod model at low ϵ is due to the fact that the analytic spring force law model assumes *continuous* random walk whereas in real bead-rod chains they undergo *discrete* random walks in N steps. Therefore for ϵ less than one Kuhn length the real chains are excluded from the region between the bead and the wall and have zero probability of residing in that region, while in the continuous random walk model, the bead-spring demonstrates nonzero probability of finding chain segments there. Therefore the bead-spring model is slightly erroneous in such cases. In the presence of one wall, this error is significant only for small ϵ and is negligible for most cases, but this error does pose problems in descriptions of chains between two walls as will be shown below.

C. Effect of two walls on the entropic spring force law

In the presence of two walls, we have infinite reflections of mirror images of point B both above the upper wall and below the lower wall as shown in Fig. 5(b). Therefore we have the following expression for the probability and entropic spring force:

$$P_{2w}(Q) = P(Q) + \sum_{i=1} (-1)^i [P(Q_i) + P(Q_{-i})], \tag{16}$$

$$F_{2w}(Q) = -kT \frac{\partial \ln P_{2w}(Q)}{\partial Q}, \tag{17}$$

where the index for Q in the summation of Eq. (16) is positive for reflections above the upper wall and negative for reflections below the lower wall. Since the probability of finding an extension greater than the chain's contour length is zero, the summation is

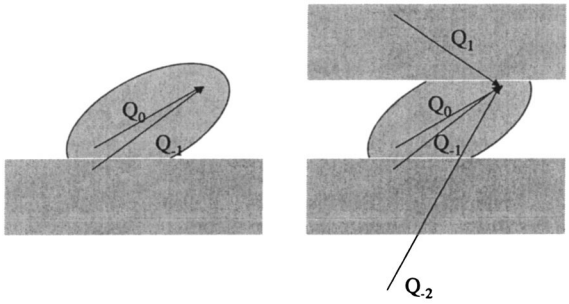

FIG. 5. To obtain the correct force law, one reflection is needed in the presence of a single wall [shown on the left (a)] and multiple reflections in the case of two walls [shown on the right (b)]. Only the first two reflections from each wall are shown for the two-wall case.

truncated at a finite value where Q_i exceeds maximum extension of the chain. In the limit of the gap width H going to zero, we should recover the 2D force law.

If we consider the same orientations of the chain as those shown in Fig. 3(a) we expect that for the chain stretched in the direction parallel to the confining walls and placed at the center of the channel ($y = H/2$), $F_{\|}$ should approach the 2D force law as gap width H tends toward zero. As was seen in Sec. III B, even though the correction for each reflection is small, the cumulative effect is finite and we expect the force to approach 2/3 of the 3D force law in small extensions and 1/2 of the 3D force law at large extensions [more precisely the ratio approaches $(2-Q^2)/(3-Q^2)$] [Woo (2003)]. As gap width H is decreased, the thin gap entropic spring force approaches 2D force but at small enough gap width it deviates from its expected 2D value considerably as shown in Fig. 6(a). On the other hand, the bead-rod model gives the correct limiting force law behavior. The failure of the bead-spring model to mimic the bead-rod model will be discussed below. For the chain stretched perpendicular to the confining walls placed halfway ($y = H/2$) in the channel [Fig. 3(b)], we find the force diverges as ϵ approaches 0 as shown in Fig. 6(b).

The random walk problem is equivalent to a transient diffusion equation with a delta function source in the limit of $N \to \infty$ and small deformation, that is, in the Hookean limit. In the presence of the impenetrable walls, one can expand the solution to the transient diffusion equation in terms of the eigenfunctions of the diffusion operator and find a series solution that satisfies the boundary condition that the probability of finding a chain segment at the wall is zero [Carslaw and Jaeger (1959); Doi and Edwards (1986)]. The resulting force law is different from the one without confinement and this new force diverges near the wall as $1/\epsilon$ where ϵ is the distance from the wall. Therefore the confining wall plays a role that is analogous to that of the finite extensibility of the chain even for linear spring force models and the divergence near the wall for both linear Hookean and nonlinear spring force law is shown in Fig. 6(b). But, as mentioned in Sec. III B, very near the wall, the continuous approximation fails and the discrete nature of the random walk becomes important. This gives rise to abnormal force law behavior in extreme confinement for bead-spring models. As shown in Fig. 6(a) the bead-spring model with large N (a more coarsely grained model) fails to predict the universal force law at extreme confinement.

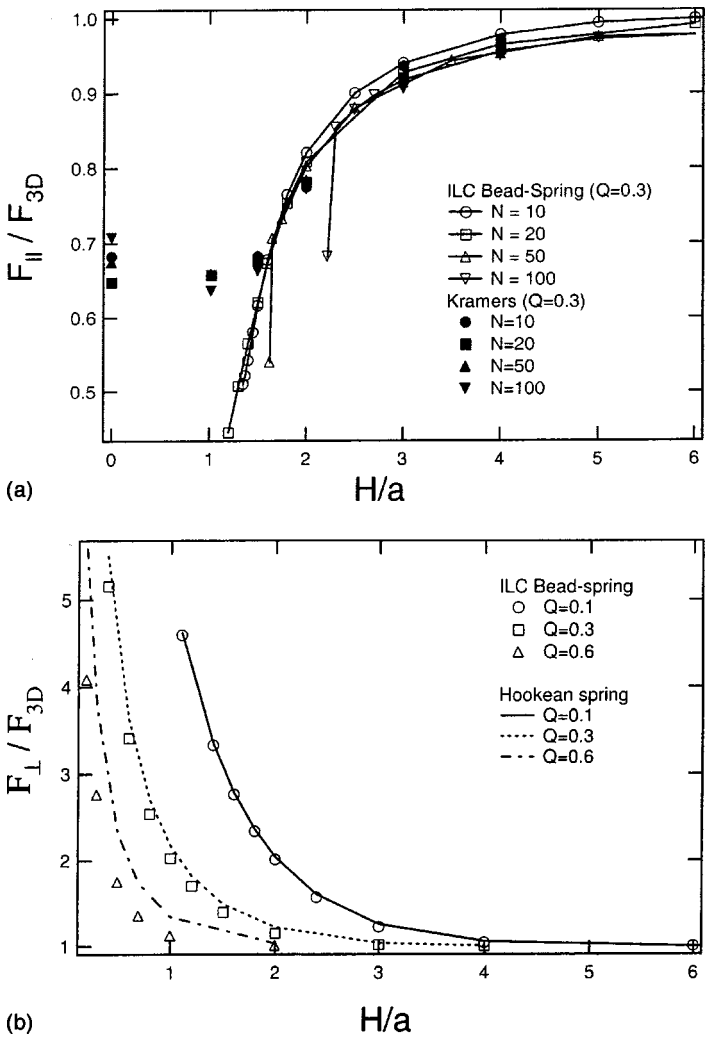

FIG. 6. Comparison of bead-rod force law with bead-spring force at various extensions as a function of gap width H. The chain is placed halfway between the walls. (a) Force for the chain oriented parallel to the confining walls at $Q = 0.3$. (b) Comparison between linear Hookean spring and nonlinear ILC for the chain oriented perpendicular to the confining walls.

D. Master curve for the entropic spring force in thin gaps

The abnormal behavior of the entropic spring force law in extreme confinement becomes worse when more coarsely grain models [i.e., ones with larger extensibility parameter b] are used. At $Q = 0.3$ for the most finely grain model of $b = 30$ (or equivalently $N = 10$) the force law curve follows the exact bead-rod force law up to 1.5 Kuhn step length and then instead of asymptoting to the 2D value, continues to fall well below it. When more coarsely grained models (bead spring with larger b) are used, the simulations fail to predict the correct force law at much larger gap widths as shown in Fig. 6(a). Therefore, generating wall reflections of the entropic spring force law is not a valid approximation everywhere and special care must be taken for small gap widths. Here we suggest a remedy for avoiding this: Since the most finely grained model of $b = 30$ is able to capture the correct thin gap spring force above some small critical gap width, we

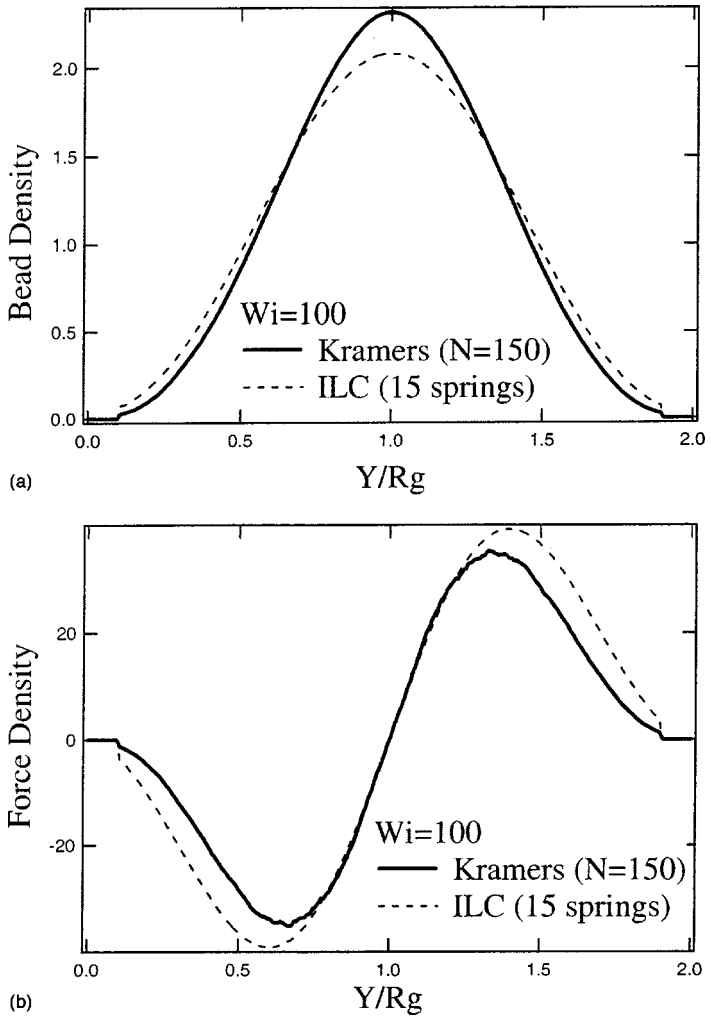

FIG. 7. Comparison of density profiles of the bead rod and bead spring using the correct thin gap bead-spring force law at $Wi = 100$. (a) Bead density profile. (b) Force density profile.

postulate that the force law defined by this most finely grained model is the master curve for all gaps above the critical. If this curve predicts force that is smaller than the 2D limiting behavior, we set the force to the 2D force. Therefore the final, composite master curve can predict the correct thin gap force at all gap widths. This master curve can then be used for force parallel to the walls ($F_{\parallel}$) where significant deviation from the bead-rod chain occurs. For force perpendicular to the walls ($F_{\perp}$), the deviation is negligible and we can use Eq. (17). As shown in Fig. 6(b), near the wall, the force perpendicular to the confining walls ($F_{\perp}$) increasingly repels the chain from the wall. Therefore the 3D entropic spring force overpredicts the chain density near the wall compared to the correct thin gap force (Fig. 1). When the *correct* thin gap force law is used the comparison with the bead-rod result is much better and for a very flexible chain with $N = 150$ we find excellent agreement between the bead-rod and bead-spring chains in both density profiles except for slight overprediction of the force density near the wall (Fig. 7).

IV. ALGORITHM FOR BEAD-SPRING MODELS IN THIN GAPS

In a previous paper [Somasi *et al.* (2002)], we proposed a second-order predictor-corrector-based algorithm for Brownian dynamics simulation of three popular nonlinear multibead-spring models (FENE chain, worm-like chain, and Cohen–Padé approximation to the inverse Langevin chain) in unbound flow. The algorithm was further extended to simulate bead-spring chains with anisotropic drag on each bead in a confined geometry [Woo (2003)]. In this case, the presence of the confining wall both increases the drag and makes it anisotropic. If the drag coefficient is not a constant, artificial drift arises from the regions of low drag to regions of high drag [Grassia *et al.* (1995)]. To avoid this aphysical drift which tends to make chains accumulate near the wall, one can either explicitly include a drift correction term to the stochastic differential equation or use either a first-order midpoint or higher order algorithm to solve the stochastic differential equation for chain dynamics [Grassia *et al.* (1995)]. Since our algorithm is second order we do not need to explicitly include a drift correction term. We emphasize within this context that use of a first-order Euler scheme with configuration-dependent drag in thin gap flow without including the drift results in a highly erroneous chain density profile and consequently incorrect interfacial rheology. Details of the algorithm for thin gap flow can be found elsewhere [e.g., see Woo (2003)].

V. HYDRODYNAMIC INTERACTION WITH THE WALL

The consequence of confinement is not only that of changing the entropic force law through the change in configurational space of the chain. To demonstrate this we have performed simulations with the correct entropic spring force law in the channel that correspond to the experiment conducted by Bakajin *et al.* (1998) in which a DNA chain is hooked on a post under flow driven by an electric field and subsequently allowed to relax from the extended state to its equilibrium coiled state. This experiment was conducted with varying gap widths to study the effect of confinement. In our simulation we find that employing the correct entropic force law alone is not enough to capture the quantitative difference in relaxation process at various degrees of confinement. The *hydrodynamic interaction* (HI) *of the chain with the wall* is found to be important as was also suggested by Bakajin *et al.* (1998).

In their experiment, Bakajin *et al.* (1998) used T4 DNA which has a contour length of 74 μm and persistence length of 65 nm. This corresponds to about 600 Kuhn steps in the chain and we have modeled this DNA using an worm-like chain with 60 springs, with each spring corresponding to 10 Kuhn steps. For the relaxation experiment with the largest gap width ($H = 5\ \mu$m, 40 Kuhn step length), we assume it to be a 3D relaxation process since the gap width is much bigger than the characteristic chain size (i.e., $Rg = 10$ Kuhn step lengths). When the gap width is smaller than 1.5 Kuhn step lengths, the entropic thin gap spring force in the direction parallel to the walls becomes the 2D entropic spring force as shown in Fig. 6(a), therefore we assume their relaxation experiment with the smallest gap width ($H = 0.09\ \mu$m or 0.7 Kuhn length) corresponds to the exact 2D relaxation in our simulation. Bakajin *et al.* (1998) found a factor of 4 increase in drag in their smallest channel ($H = 0.09\ \mu$m) compared to in their widest channel ($H = 5\ \mu$m) and therefore we set the longest relaxation time for the 2D case four times that of the 3D case, since the relaxation time is proportional to drag on the chain. Both of these assumptions were justified by Bakajin *et al.* (1998) in their paper. Thus in Fig. 8, we find quantitative agreement for both wide gap ($H = 5\ \mu$m) and very narrow gap ($H = 0.09\ \mu$m) relaxation after fitting the increased drag on the chain.

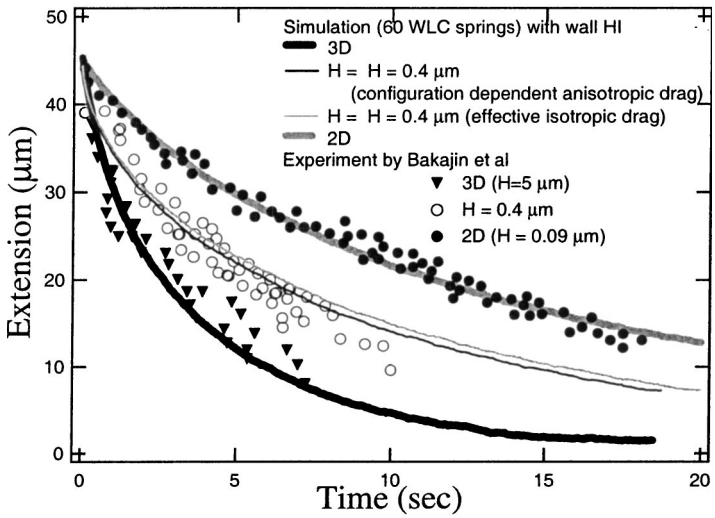

FIG. 8. Comparison of experimental results [Bakajin *et al.* (1998)] and our simulation of a chain relaxing from an extended state. At $H = 0.4\ \mu$m, one simulation run was performed with configuration-dependent anisotropic drag which varies across the gap width and another run was done with an average effective isotropic drag constant across the gap width.

Recent studies of chain dynamics in shear flow of dilute and semidilute λ-phage DNA solutions showed that chain dynamics with interchain and intrachain HI can be captured by simulations without HI as long as the overall effect of HI is taken into account in the form of increased drag on the chain [Hur *et al.* (2001)]. Simulation with longer DNA [Jendrejack *et al.* (2002)] show very small changes with HI even for chains as long as 120 μm, again as long as the overall drag on the chain is taken into account by matching the longest relaxation time. Similarly, in our problem where chains are confined between two parallel walls, the main consequence of hydrodynamic interaction of the chain with the wall is to increase drag on the chain. Since the relaxation time scales like the viscosity, and the confinement increases the viscous drag on the chain, the relaxation time increases under confinement and we were able to capture the experimental results shown in Fig. 8, once we accounted for this increase in viscous drag on the chain. We point out again that, since we consider only dilute solutions, interchain HI can be ignored, but HI between the chain and the wall remains important.

To account for the effect of HI on the chain in the confined geometry for intermediate gap widths [i.e., neither wide gap (3D) nor narrow gap (2D)] via increased drag on the chain, we consider motion of a sphere between two walls. The drag on the sphere moving parallel to a *single wall* was calculated by Faxen, who found that the drag increases by a factor of

$$\beta_{\parallel}^{1w}(y) = \left[1 - \frac{9}{16}\left(\frac{a}{y}\right) + \frac{1}{8}\left(\frac{a}{y}\right)^3 - \frac{45}{256}\left(\frac{a}{y}\right)^4 - \frac{1}{16}\left(\frac{a}{y}\right)^5\right]^{-1}, \tag{18}$$

where a is the radius of the sphere and y is the distance from the wall [Happel and Brenner (1965)].

For a sphere moving perpendicular to a single wall, the correction factor was calculated by Lorentz and Brenner [Brenner (1961); Happel and Brenner (1965)] and the drag increases by a factor of

$$\beta_{\perp}^{1w}(y) = \frac{4}{3}\sinh\alpha \sum_{i=0}^{\infty}\left[\frac{i(i+1)}{(2i-1)(2i+3)}\left(\frac{2\sinh(2i+1)\alpha+(2i+1)\sinh 2\alpha}{4\sinh^2(i+1/2)\alpha-(2i+1)^2\sinh^2\alpha}-1\right)\right], \tag{19}$$

where $\alpha = \cosh^{-1}(y/a)$.

In a similar way, drag correction in the presence of *two walls* can be carried out by the superposition of two single-wall effects and is given by [Grasselli and Lobry (1997)]

$$\beta_{\parallel}^{2w} = 1+\sum_{i=0}^{\infty}(\beta_{\parallel}^{1w}(y+iH)-1)+\sum_{i=0}^{\infty}(\beta_{\parallel}^{1w}(iH-y)-1)-2\sum_{i=0}^{\infty}(\beta_{\parallel}^{1w}(iH)-1), \tag{20}$$

where y is the distance from the either of the two walls. The same expression holds for $\beta_{\perp}^{2w}$ as well.

The first two summation terms are reflection terms from the upper and lower walls, respectively, and the third summation term is the interaction between the two walls. The above expression was originally derived for the case of motion perpendicular to walls but can also be used for motion parallel to walls as well since, compared to experimental results, it is found to be accurate for both cases [Lobry and Ostrowsky (1996); Lin *et al.* (2000)].

We now wish to simulate the relaxation process for the intermediate gap width ($H = 0.4\,\mu$m), shown in Fig. 8. To do this, we consider the effect of wall HI in two different ways: In the first approach, we explicitly simulate a bead-spring chain with *configuration dependent drag* using the *anisotropic* drag expression given by Eq. (20). In the second approach, we replaced the effect of the wall HI with increased *effective isotropic* drag instead of position-dependent anisotropic drag. Since drag is a function of the distance from the wall, we obtained the chain segmental density profile from the Brownian dynamics with *isotropic drag* at equilibrium at a given gap width and the effective drag is calculated from the weighted average as

$$\langle\beta_{\parallel}\rangle = \int_0^H \rho(y)\beta_{\parallel}^{2w}(y)dy \Big/ \int_0^H \rho(y)dy. \tag{21}$$

In comparison to the experiment we use drag parallel to the confining walls $\beta_{\parallel}^{2w}$, since the relaxation process occurs in that plane. From Eq. (21), we get $\langle\beta_{\parallel}\rangle = 1.5$ at gap width of 0.4 μm, which is consistent with the scaling argument used by Bakajin *et al.* The relaxation of extended chains is shown in Fig. 8, and it shows excellent agreement between experiment and simulation for $H = 0.4\,\mu$m when one uses the exact configuration-dependent anisotropic drag [Eq. (20)] which takes the wall HI into account explicitly. Similarly, if we use the *average* effective isotropic drag [Eq. (21)], we get excellent agreement with the experiment. Note that excellent agreement with experiment is found even though no adjustable parameters are used, i.e., only the longest relaxation time from the 3D experiment was used to determine the coefficients multiplying Eq. (20) in the drag expression.

VI. CONCLUSIONS

In this study we have presented a self-consistent multiscale simulation technique for flow of dilute flexible polymeric solutions in confined channels. In confined channel flow the presence of walls changes the configurational space of the chain considerably, and results in a significantly different entropic spring force law compared to the 3D case. The bead-rod chain as a Kuhn step level model does not suffer from incorrect description

of the entropic spring force law under confinement as do bead-spring models. But due to the high computational cost, only a certain class of problems can be solved using bead-rod models. Therefore, we have developed an efficient algorithm for dynamic simulation of bead-spring chains with the corrected entropic spring force law which reduces to 3D force law in wide gaps and to 2D force law in narrow gaps. Finally, we have found that the hydrodynamic interaction with the wall is important in thin gap flow and its main consequence is to increase viscous drag on the chain. In Part II we present the effect of corrected entropic spring force laws and wall HI on DNA chain dynamics and solution rheology in microchannel flows.

ACKNOWLEDGMENT

Two of the authors (E.S.G.S. and B.K.) would like to thank the National Science Foundation for supporting this work through Grant Nos. CTS-9731896-002 and CTS-97325535, respectively.

References

Abramowitz, M., and I. A. Stegun, *Handbook of Mathematical Functions with Formulas, Graphs, and Mathematical Tables* (Wiley–Interscience, New York, 1984).

Allegra, G., and E. Colombo, ''Polymer chain between attractive walls: A second-order transition,'' J. Chem. Phys. **98**, 7398–7404 (1993).

Aubert, J. H., and M. Tirrel, ''Effective viscosity of dilute polymer solutions near confining boundaries,'' J. Chem. Phys. **77**, 553–561 (1982).

Ausserre, D., J. Edwards, J. Lecourtier, H. Hervet, and F. Rondelez, ''Hydrodynamic thickening of depletion layers in colloidal solutions,'' Europhys. Lett. **14**, 33–38 (1991).

Babcock, H. P., D. E. Smith, J. S. Hur, E. S. G. Shaqfeh, and S. Chu, ''Relating the microscopic response of a polymeric fluid in a shear flow,'' Phys. Rev. Lett. **85**, 2018–2021 (2000).

Bakajin, O. B., T. A. J. Duke, C. F. Chou, S. S. Chan, R. H. Austin, and E. C. Cox, ''Electrohydrodynamic stretching of DNA in confined environments,'' Phys. Rev. Lett. **80**, 2737–2740 (1998).

Brenner, H., ''The slow motion of a sphere through a viscous fluid towards a plane surface,'' Chem. Eng. Sci. **16**, 242–251 (1961).

Brunn, P. O., ''The effect of a solid wall for the flow of dilute macromolecular solutions,'' Rheol. Acta **15**, 23–29 (1976).

Brunn, P. O., and S. Grisafi, ''Wall effects in simple shear of dilute polymer solutions: Exact results for very narrow and very wide channels,'' J. Non-Newtonian Fluid Mech. **24**, 343–363 (1987).

Carslaw, H. S., and J. C. Jaeger, *Conduction of Heat in Solids*, 2nd ed. (Clarendon, New York, 1959).

Chopra, M., and R. G. Larson, ''Brownian dynamics simulations of isolated polymer molecules in shear flow near adsorbing and nonadsorbing surfaces,'' J. Rheol. **46**, 831–862 (2002).

de Pablo, J. J., H. C. Öttinger, and Y. Rabin, ''Hydrodynamic changes of the depletion layer of dilute polymer solutions near a wall,'' AIChE J. **38**, 273–283 (1992).

DiMarzio, E. A., ''Proper accounting of conformations of a polymer near a surface,'' J. Chem. Phys. **42**, 2101–2104 (1965).

Doi, M., and S. F. Edwards, *The Theory of Polymer Dynamics* (Oxford University Press, New York, 1986).

Doyle, P. S., E. S. G. Shaqfeh, and A. P. Gast, ''Dynamic simulation of freely-draining, flexible polymers in steady linear flows,'' J. Fluid Mech. **334**, 251–291 (1997a).

Doyle, P. S., E. S. G. Shaqfeh, and A. P. Gast, ''Rheology of ''wet'' polymer brushes via Brownian dynamics simulation: Steady vs oscillatory shear,'' Phys. Rev. Lett. **78**, 1182–1185 (1997b).

Duering, E., and Y. Rabin, ''Polymers in shear flow near repulsive boundaries,'' Macromolecules **23**, 2232–2237 (1990).

Duering, E., and Y. Rabin, ''Polymers in plane Poiseuille flow: Dynamic Monte Carlo simulation,'' J. Rheol. **35**, 213–219 (1991).

Feller, W., *An Introduction to Probability Theory and Its Applications*, 2nd ed. (Wiley, New York, 1961).

Graessley, M. W., R. L. Hayward, and G. S. Grest, ''Excluded-volume effects in polymer solutions. 2. Comparison of experimental results with simulation data,'' Macromolecules **32**, 3510–3517 (1999).

Grasselli, Y., and L. Lobry, ''Hydrodynamic interactions between a particle and two rigid walls: Effect of surface roughness and many-body hydrodynamic interactions,'' Phys. Fluids **9**, 3929–3931 (1997).

Grassia, P. S., E. J. Hinch, and L. C. Nitsche, ''Computer simulation of Brownian motion of complex systems,'' J. Fluid Mech. **282**, 373–403 (1995).

Happel, J., and H. Brenner, *Low Reynolds Number Hydrodynamics* (Prentice–Hall, Englewood Cliffs, NJ, 1965).

Herrchen, M., and H. Öttinger, ''A detailed comparison of various FENE dumbbell models,'' J. Non-Newtonian Fluid Mech. **68**, 17–42 (1997).

Ho, C. M., and Y. C. Tai, ''Review: MEMS and its applications for flow control,'' J. Fluids Eng. **118**, 437–447 (1996).

Ho, C. M., and Y. C. Tai, ''Micro-Electro-Mechanical-Systems (MEMS) and fluid flows,'' Annu. Rev. Fluid Mech. **30**, 579–612 (1998).

Hur, J. S., E. S. G. Shaqfeh, and R. G. Larson, ''Brownian dynamics simulations of single DNA molecules in shear flow,'' J. Rheol. **44**, 713–742 (2000).

Hur, J. S., E. S. G. Shaqfeh, H. P. Babcock, D. E. Smith, and S. Chu, ''Dynamics of dilute and semidilute DNA solutions in the startup of shear flow,'' J. Rheol. **45**, 421–450 (2001).

Jendrejack, R. M., J. J. de Pablo, and M. D. Graham, ''Stochastic simulations of DNA in flow: Dynamics and the effects of hydrodynamic interactions,'' J. Chem. Phys. **116**, 7752–7759 (2002).

Koch, D. L., and J. F. Brady, ''The effective diffusivity of fibrous media,'' AIChE J. **32**, 575–591 (1986).

Kuhn, W., and F. Grün, ''Relationships between elastic constants and stretching double refraction of highly elastic substances,'' Kolloid-Z. **101**, 248–253 (1942).

Lee, G. B., S. H. Chen, G. R. Huang, W. C. Sung, and Y. H. Lin, ''Microfabricated plastic chips by hot embossing methods and their applications for DNA separation and detection,'' Sens. Actuators B **75**, 142–148 (2001).

Lin, B., J. Yu, and S. Rice, ''Direct measurements of constrained Bronwnian motion of an isolated sphere between two walls,'' Phys. Rev. E **62**, 3909–3919 (2000).

Lobry, L., and N. Ostrowsky, ''Diffusion of Brownian particles trapped between two walls: Theory and dynamic-light-scattering measurements,'' Phys. Rev. B **53**, 12050–12056 (1996).

Maier, B., and J. O. Radler, ''Conformation and self-diffusion of single DNA molecules confined to two dimensions,'' Phys. Rev. Lett. **82**, 1911–1914 (1999).

Marko, J. F., and E. D. Siggia, ''Stretching DNA,'' Macromolecules **28**, 3427–3433 (1995).

Mavrantzas, V. G., and A. N. Beris, ''Theoretical study of wall effects on the rheology of dilute polymer solutions,'' J. Rheol. **36**, 175–213 (1992).

Mavrantzas, V. G., and A. N. Beris, ''A hierarchical model for surface effects on chain conformation and rheology of polymer solutions. II. Application to a neutral surface,'' J. Chem. Phys. **110**, 628–638 (1999).

Muller-Mohnssen, H., D. Weiss, and A. Tippe, ''Concentration dependent changes of apparent slip in polymer solution flow,'' J. Rheol. **34**, 223–244 (1990).

Muthukumar, M., ''Brownian dynamics of polymer chains in membranes,'' J. Chem. Phys. **82**, 5696–5706 (1999).

Öttinger, H. C., *Stochastic Processes in Polymeric Fluids* (Springer, New York, 1996).

Rowley, R. L., *Statistical Mechanics for Thermophysical Property Calculations* (Prentice–Hall, Englewood Cliffs, NJ, 1994).

Schiek, R. L., and E. S. G. Shaqfeh, ''A nonlocal theory for stress in bound, Brownian suspensions of slender, rigid fibres,'' J. Fluid Mech. **296**, 271–324 (1995).

Smith, D. E., H. P. Babcock, and S. Chu, ''Single polymer dynamics in steady shear flow,'' Science **283**, 1724–1727 (1999).

Smith, S. B., L. Finzi, and C. Bustamante, ''Direct mechanical measurements of the elasticity of single DNA molecules by using magnetic beads,'' Science **258**, 1122–1126 (1992).

Somasi, M., B. Khomami, N. J. Woo, J. S. Hur, and E. S. G. Shaqfeh, ''Brownian dynamics simulation of bead-rod and bead-spring chains: Numerical algorithms and coarse graining issues,'' J. Non-Newtonian Fluid Mech. **108**, 227–255 (2002).

Woo, J. H., DNA chain dynamics and its applications to micro-devices and scission, Ph.D. thesis (Stanford University, Stanford, CA, 2003).